

Observation of superspin-glass behavior in Fe_3O_4 nanoparticles

Masatsugu Suzuki,* Sharbani I. Fullem, and Itsuko S. Suzuki

Department of Physics, State University of New York at Binghamton, Binghamton, New York 13902-6000

Lingyan Wang and Chuan-Jian Zhong

Department of Chemistry, State University of New York at Binghamton, Binghamton, New York 13902-6000

(Dated: June 4, 2021)

The aging and memory effects of Fe_3O_4 nanoparticles have been studied using a series of zero-field cooled (ZFC) and field-cooled (FC) magnetization measurements at various aging protocols. The genuine ZFC magnetization after the ZFC procedure with a single stop and wait process shows an aging dip at the stop temperature on reheating. The depth of the aging dip is dependent on the wait time. The frequency dependence of the AC magnetic susceptibility is indicative of critical slowing down at a freezing temperature T_f ($= 30.6 \pm 1.6$ K). The relaxation time τ is described by a power law form with a dynamic critical exponent x ($= 8.2 \pm 1.0$) and a microscopic relaxation time τ_0 [$= (1.33 \pm 0.05) \times 10^{-9}$ sec]. The ZFC-peak temperature decreases with increasing magnetic field (H), forming a critical line with an exponent $p = 1.78 \pm 0.26$, close to the de Almeida-Thouless exponent ($p = 3/2$). These results indicate that the superspin glass phase occurs below T_f .

PACS numbers: 75.50.Lk, 75.50.Tt, 75.30.Cr

I. INTRODUCTION

The aging and memory effects of ferromagnetic nanoparticles have been the focus of extensive studies in recent years.^{1,2,3,4,5,6,7,8,9,10,11,12,13} Each ferromagnetic nanoparticle has a large magnetic moment (so-called superspin). Depending on the interactions between superspins, these systems are classed into two types. The non-interacting superspins give rise to superparamagnetic behavior. The superspins thermally fluctuate between their easy directions of magnetization and freeze along these directions at the blocking temperature T_b , where the relaxation time τ becomes equal to the measuring time τ_m . Thus the superparamagnet (SPM) has a ferromagnetic blocked state below T_b . The relaxation time typically obeys an Arrhenius law. When the interactions between superspins, which are fully frustrated and random, become sufficiently strong, the interacting superspins cause spin frustration effect, resulting in superspin glass (SSG) behavior below a freezing temperature T_f . The low temperature spin-glass (SG) phase is experimentally characterized by observation of the flatness of the FC susceptibility below T_f , a critical slowing down of the relaxation time τ from the AC magnetic susceptibility, and a divergent behavior of the nonlinear susceptibility.^{3,7} The relaxation time τ which can be determined from the shift of the peak temperature of the AC magnetic susceptibility χ' (dispersion) vs temperature (T) curve with frequency, exhibits a critical slowing down for SSG's.^{2,6}

The non-equilibrium properties of SSG's and SPM's have been observed in various nanoparticle systems, as a wait time dependence of zero-field cooled (ZFC) and field cooled (FC) magnetizations under various cooling protocols.^{1,2,4,5,6,8,9,10,11,12,13} The aging and memory effects of the SSG's are rather different from those of SPM's. A broad distribution of relaxation times characterize SPM's, while a critical slowing down occurs in

the SSG's. The main features of their aging and memory effects are summarized as follows. These features provide a very unique method to determine dynamics governed by spin correlations between nanoparticles in SSG's and SPM's (Sasaki et al.¹²).

(1) (Genuine ZFC measurement). Only for SSG's, the ZFC magnetization M_{ZFC} shows an aging dip at a stop temperature on reheating after the ZFC protocol with a single stop and wait process. The depth of the aging dip depends on the wait time t_w .^{8,10,12}

(2) (Genuine FC measurement). For both SSG's and SPM's, the memory effect of M_{FC} during a FC protocol with intermittent stop and wait processes are observed. A decrease of M_{FC} is observed with decreasing T for SSG's, while an increase of M_{FC} is observed with decreasing T for the SPM's.^{9,11,12,13}

(3) (ZFC relaxation rate). Only for SSG's, the corresponding relaxation rate $S_{ZFC}(t, t_w)$ [$= (1/H)dM_{ZFC}/d\ln t$] has a peak around $t = t_w$, as observed in spin glasses (aging effect).^{1,5,8}

In the present work, we have studied the magnetic properties of Fe_3O_4 nanoparticles. Synthesis and characterization of Fe_3O_4 nanoparticles used in the present work has been reported in detail previously.^{14,15} A simple review on the sample characterization will be presented in Sec. II. We have measured the ZFC susceptibility (χ_{ZFC}), FC susceptibility (χ_{FC}) and AC magnetic susceptibility (χ' , χ'') of Fe_3O_4 nanoparticles at various cooling protocols using a SQUID (superconducting quantum interference device) magnetometer. We show that the aging and memory effects, critical slowing down, and the flatness of the FC susceptibility at low temperatures, are clearly observed in Fe_3O_4 nanoparticles. These results indicate that the SSG phase occurs below a spin freezing temperature T_f ($= 30.6 \pm 1.6$ K).

The H - T diagrams are examined from the temperature dependence of χ_{ZFC} and χ_{FC} of Fe_3O_4 nanoparticles at

various H . The peak temperatures of the ZFC susceptibility of this system is determined as a function of H . We show that the ZFC-peak temperature T_p ($= T_f$) for Fe_3O_4 nanoparticles decreases with increasing H , forming a critical line with an exponent $p = 1.78 \pm 0.26$, close to the de Almeida-Thouless (AT) exponent ($= 3/2$).¹⁶ This critical line is the phase boundary between the SPM and SSG phases. These results can be well described by the SSG model of interacting Fe_3O_4 nanoparticle systems.

The contents of the present paper are as follows. In Sec. II experimental procedure is presented, including the characterization of Fe_3O_4 nanoparticles. In Sec. III we present experimental results on the ZFC susceptibility, FC susceptibility, and AC susceptibility of our systems under various cooling protocols. In Sec. IV, the AT exponent p will be discussed.

II. EXPERIMENTAL PROCEDURE

Fe_3O_4 nanoparticles capped with mixed monolayer of oleic acid and oleylamine were synthesized using a modified protocol.^{14,15} Briefly, 0.71 g $\text{Fe}(\text{acac})_3$ (2 mmol) was mixed with 2 mL oleic acid (~ 6 mmol), 2 mL oleylamine (~ 6 mmol), and 2.58 g 1,2-hexadecanediol (10 mmol) in 20 mL phenyl ether under argon atmosphere with vigorous stirring. The solution was heated to 210 °C and refluxed for 2 hrs. After cooling to room temperature, ethanol was added into the solution. A dark-brown precipitate (Fe_3O_4 nanoparticles) was separated by centrifuging, followed by washing with ethanol and drying with nitrogen. The sample for this study was used as synthesis.

Transmission electron microscopy (TEM) result for Fe_3O_4 nanoparticles shows the particles displayed high monodispersity in size ($52 \pm 5 \text{ \AA}$) and well isolated, which is characteristic of the presence of an organic shell on the particle surface.^{14,15} In domains with densely-packed nanoparticles in the TEM image, we can determine the average edge-to-edge distance ($\sim 20 \text{ \AA}$), which was found to be quite close to the value expected for interdigitation of the alkyl chains in the interparticle shells.¹⁴ The X-ray Powder Diffraction (XRD) patterns show that the nanoparticles are highly crystalline materials.^{14,15} The crystalline features are reflected by the excellent matching of the diffraction peaks with that for standard spectra of Fe_3O_4 . The Thermogravimetry Analysis (TGA) data for Fe_3O_4 nanoparticles capped with mixed monolayer revealed a mass loss of $\sim 32\%$ for the organic shell, so the mass percentage of Fe_3O_4 in the sample (filling factor) is about 68%.¹⁴ The further detail of Fe_3O_4 nanoparticle synthesis and characterization were given in previous reports.^{14,15}

The DC magnetization and AC magnetic susceptibility were measured using a SQUID magnetometer (Quantum Design, MPMS XL-5). Before the measurements, a possible remnant magnetic field was removed using ultra

low field option at 298 K: the resultant remnant field was less than 3 mOe. The measurements of the DC magnetization and AC magnetic susceptibility were carried out after appropriate cooling procedures. The details of the cooling protocol for each measurement are described in Sec. III and respective figure captions.

III. EXPERIMENTAL RESULT

A. Curie-Weiss constant and saturation magnetization

The DC magnetic susceptibility at $H = 1$ kOe was measured as a function of T for $150 \leq T \leq 298$ K. It exhibits a well-defined Curie-Weiss behavior with a Curie-Weiss constant, $C_g = 11.39 \pm 0.30$ (emu K/g). The magnetization M at both $T = 5.0$ and 100 K was also measured as a function of H for $0 \leq H \leq 45$ kOe. The magnetization M saturates to a saturation magnetization M_s ($= 63.97$ emu/g) above 20 kOe. The composition of the bulk Fe_3O_4 is described by $\text{FeO} \cdot \text{Fe}_2\text{O}_3$. The ferric (Fe^{3+}) ions are in a state with spin $S = 5/2$, while the ferrous (Fe^{2+}) ions are in a state with spin $S = 2$. The bulk Fe_3O_4 is a ferrimagnet with the Curie temperature 858 K. The spin magnetic moment of the Fe^{3+} ions in the tetrahedral A sites are antiparallel to that in the octahedral B site. Then the magnetic moment of the Fe^{3+} ions cancel out, leaving only the magnetic moment of the Fe^{2+} ions in the octahedral B site.^{17,18} This means that there is one Fe^{2+} mole per a molar mass m_0 ($= 231.54$ g) for one Fe_3O_4 mole.

The average diameter of Fe_3O_4 nanoparticles is evaluated using using the data of the Curie-Weiss constant and the saturation magnetization in the following way. We assume that the mass ratio of Fe_3O_4 nanoparticles to the total sample is given by f . The parameter f is the filling factor of Fe_3O_4 nanoparticles over the whole system^{14,15} and can be determined from the saturation magnetization M_s . The molar saturation magnetization M_{s0} (emu/ Fe^{2+} mole) for the system is evaluated as

$$M_{s0} = (m_0 M_s) / f = 1.481 \times 10^4 / f \text{ (emu/Fe}^{2+} \text{ mole)}, \quad (1)$$

which is equal to the molar saturation magnetization \bar{M}_s for Fe^{2+} spins given by

$$\bar{M}_s = N_A g \mu_B S = 2.368 \times 10^4 \text{ (emu/Fe}^{2+} \text{ mole)}. \quad (2)$$

where N_A is the Avogadro number, μ_B is the Bohr magneton, g ($= 2.12$) is the Landé g -factor of Fe^{2+} ion for the bulk Fe_3O_4 ,¹⁹ and S ($= 2$) is a spin of Fe^{2+} ion. From Eqs.(1) and (2), the parameter f can be estimated as $f = 0.625$. This value of f is in good agreement with that determined from TGA ($f = 0.68$).¹⁴ The molar Curie Weiss constant C_M is given by

$$C_M = (m_0 C_g) / f = (2640 \pm 70) / f \text{ (emu K/Fe}^{2+} \text{ mole)}. \quad (3)$$

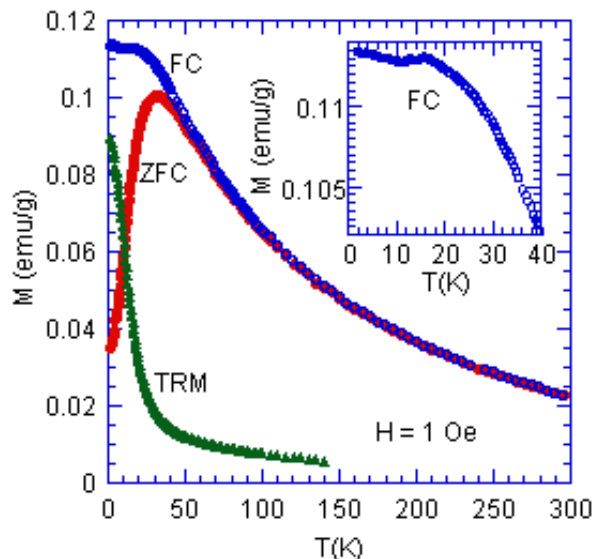


FIG. 1: (Color online) T dependence of M_{ZFC} , M_{FC} , and M_{TRM} for Fe_3O_4 nanoparticles. $H = 1$ Oe. The detail of the ZFC, FC, and TRM procedures is given in the text. The detail of M_{ZFC} vs T at $H = 1$ Oe at low T is shown in the inset.

Then the average number N_0 of Fe^{2+} atoms (which is also equal to the number of Fe_3O_4 molecules) in each nanoparticle can be estimated as

$$N_0 = (R/a_0)^3 = C_M/\bar{C}_M = (780 \pm 20)/f, \quad (4)$$

where \bar{C}_M is the molar Curie-Weiss constant for the free Fe^{2+} spins, R is the average radius of Fe_3O_4 nanoparticles, $a_0 (= 2.63\text{\AA})$ is the average radius of the sphere with the same volume occupied by one Fe_3O_4 molecule, and is defined by $a_0 = [3m_0/(4\pi\rho N_A)]^{1/3}$, $\rho (= 5.21 \text{ g/cm}^3)$ is the density of bulk Fe_3O_4 . The molar Curie-Weiss constant \bar{C}_M for Fe^{2+} ions is given by $\bar{C}_M = N_A\mu_B^2 g^2 S(S+1)/3k_B = 3.371$ (emu/ Fe^{2+} mole K). From Eq.(4), the diameter d of nanoparticles can be evaluated as

$$d = 2R = 2a_0[(780 \pm 20)/f]^{1/3}. \quad (5)$$

The diameter d can be estimated as $d = 56 \pm 5\text{\AA}$ for $f = 0.625$ determined from the magnetization, and $d = 55 \pm 5\text{\AA}$ for $f = 0.680$ determined from TGA. These values are close to the ones obtained from the TEM micrograph; $d = 52 \pm 5\text{\AA}$.^{14,15}

B. ZFC, FC and TRM magnetization

Figure 1 shows the T dependence of the ZFC, FC, and thermoremanent (TRM) magnetization for Fe_3O_4 nanoparticles. These protocols used in the present work are explained as follows. (i) ZFC protocol: after the system was annealed at 298 K in the absence of H , it was

cooled rapidly from 298 to 2.0 K. Immediately after the magnetic field $H (= 1$ Oe) was turned on at 2.0 K, the ZFC magnetization was measured with increasing T from 2.0 K to 298 K. (ii) FC protocol: After the system was annealed at 298 K in the presence of H , the FC magnetization was measured with decreasing T . (iii) TRM protocol: after the system was cooled from 298 to 2.0 K in the presence of H , the magnetic field was turned off. The TRM magnetization was then measured with increasing T from 2.0 to 100 K in the absence of H . Note that in general the T dependence of M_{ZFC} is similar for SSG's and SPM's, while the T dependence of M_{FC} is noticeably different for the two. The FC magnetization M_{FC} monotonically increases with decreasing T for SPM's, while it tends to saturate to a constant value or even tends to decrease with decreasing T for SSG's. In this sense, the T dependence of M_{FC} is a means for distinguishing between SPM's and SSG's. In the inset of Fig. 1, we show the detail of M_{FC} vs T at $H = 1$ Oe. Such a T dependence of M_{FC} is rather different from that of typical SSG. However, the slight decrease in M_{FC} with decreasing T below 16 K is indicative of the feature of M_{FC} in the SSG. We note that the present system is not an ideal SSG system.

Figures 2(a) and (b) show the T dependence of χ_{ZFC} , χ_{FC} , and $\Delta\chi [= \chi_{FC} - \chi_{ZFC}]$ for the Fe_3O_4 nanoparticles at various H . The susceptibility χ_{ZFC} at $H = 1$ Oe shows a peak at T_p (≈ 32 K) for $H = 1$ Oe. The susceptibility χ_{FC} at $H (\geq 5$ Oe) tends to saturate at low temperatures well below T_p . The difference $\Delta\chi$ gradually decreases with increasing T and starts to appear at the onset temperature of irreversibility (T_{irr}). No sharp reduction of $\Delta\chi$ to zero is observed at $T = T_{irr}$, reflecting the volume distribution of Fe_3O_4 nanoparticles across the sample. Such a rounding effect of T_{irr} in $\Delta\chi$ vs T disappears at a higher H . The TEM measurement shows that the size distribution of Fe_3O_4 nanoparticles is similar to the log-normal distribution.^{14,15} Above $H = 500$ Oe, T_{irr} is very close to T_p . The flatness of χ_{FC} below T_p and the coinciding of T_{irr} and T_p suggest that the Fe_3O_4 nanoparticles exhibit a SSG-like behavior.

C. AC magnetic susceptibility

Figures 3(a) and (b) show the T dependence of the AC magnetic susceptibility: (a) the dispersion χ' and (b) the absorption χ'' at $H = 0$. After the system was annealed at 298 K in the absence of H , it was rapidly cooled from 298 to 2.0 K. Both χ' and χ'' were measured at a fixed T ($T \geq 2.0$ K) for various frequencies between 0.1 and 1000 Hz. After each measurement, the temperature was increased by ΔT . The same measurement was then repeated at the temperature $T + \Delta T$. As shown in Fig. 3(a), χ' at $f = 0.1$ Hz shows a relatively broad peak at a peak temperature $T_p(\chi')$ ($= 32.5$ K). This peak shifts to the high- T side with increasing f : $T_p(\chi') = 38.5$ K for $f = 1$ kHz. Also, the peak height of χ' increases with increas-

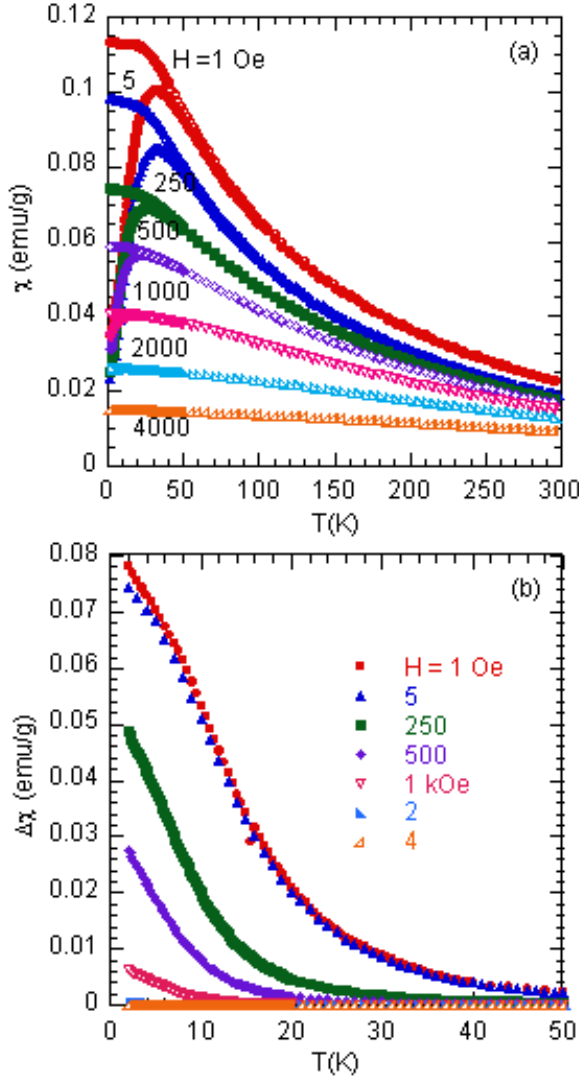


FIG. 2: (Color online) T dependence of (a) χ_{ZFC} and χ_{FC} , and (b) $\Delta\chi$ ($=\chi_{FC} - \chi_{ZFC}$) of Fe_3O_4 nanoparticles. H is changed as a parameter. $1 \text{ Oe} \leq H \leq 4 \text{ kOe}$.

ing f . As shown in Fig. 3(b), in contrast, the absorption χ'' at $f = 0.1 \text{ Hz}$ shows a relatively sharp peak at a peak temperature $T_p(\chi'')$ ($= 13.5 \text{ K}$). This peak shifts to the high- T side with increasing f : $T_p(\chi'') = 20 \text{ K}$ for $f = 1 \text{ kHz}$. The peak height of χ'' decreases with increasing f . It should be noted that χ'' is independent of f below 12 K.

It is empirically known that the frequency shift in the peak temperature $T_p(\chi')$ of χ' vs T curve, defined by $\Gamma = (1/T_p)\Delta T_p/\Delta(\log_{10}\omega)$, offers a good criterion for distinguishing SG's ($\Gamma < 0.06$) from SPM's ($\Gamma \approx 0.3$).²⁰ Our value of Γ can be estimated as $\Gamma \approx 0.05$, which suggests that our system is a SSG, and not a SPM. According to Hansen et. al.,⁶ there are two criteria for the determination of the freezing temperature. First, the freezing temperature is defined as the temperature

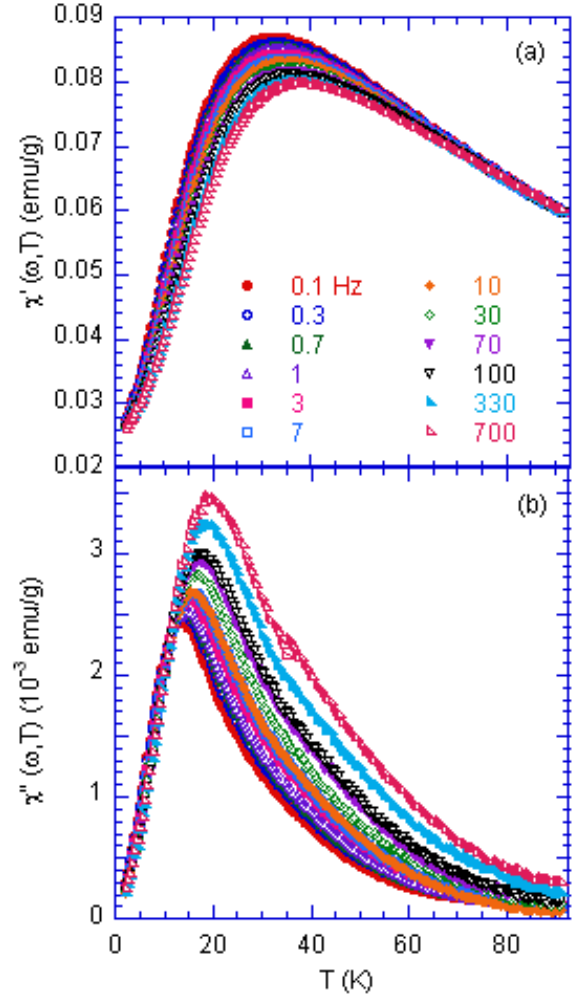


FIG. 3: (Color online) T dependence of (a) the dispersion χ' and (b) the absorption χ'' for Fe_3O_4 nanoparticles. The frequency is changed as a parameter. $f = 0.1 - 1000 \text{ Hz}$. $h = 0.5 \text{ Oe}$. $T = 2 - 100 \text{ K}$. $H = 0$.

at which χ'' attains 15% of its maximum value. Second, the freezing temperature is defined from the relation $\chi'(\omega, T_f) = 0.98\chi_{FC}(T = T_f)$. Nevertheless, for convenience here we define the freezing temperature as the peak temperature $T_p(\chi')$. Figure 4 shows the relaxation time τ which is estimated as $\tau = 1/(2\pi f)$ as a function of T [$= T_p(\chi')$]. The least-squares fit of the data of τ vs T to a power law form for the critical slowing down,

$$\tau = \tau_0(T/T_f - 1)^{-x}, \quad (6)$$

yields a dynamic critical exponent $x = 8.2 \pm 1.0$, a microscopic relaxation time $\tau_0 = (1.33 \pm 0.5) \times 10^{-9} \text{ sec}$, and a freezing temperature $T_f = 30.6 \pm 1.6 \text{ K}$. Our values of x and τ_0 are comparable with those of the Fe-C nanoparticles with a volume concentration 15 vol % (superparamagnetic) reported by Hansen et al.⁶: $x = 9.5$ and $\tau_0 = 5.0 \times 10^{-9} \text{ sec}$. Note that our value of x is also in good agreement with that of the 3D Ising spin glass

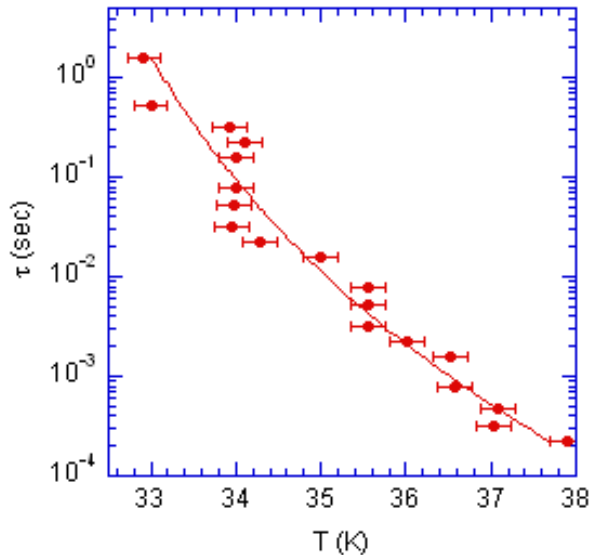


FIG. 4: (Color online) Relaxation time τ ($= 1/(2\pi f)$) vs T at various frequencies f . $f = 0.1 - 1000$ Hz. T is equal to the peak temperature $T_p(\chi')$ from χ' vs T curve. The solid line denotes a least-squares fit of the data of τ vs T to the power law form given by Eq.(6). The fitting parameters are given in the text.

$\text{Fe}_{0.5}\text{Mn}_{0.5}\text{TiO}_3$ ($x = 9.3 \pm 1.0$).²¹ These results indicate that our system is a SSG.

D. Memory effect in FC magnetization

We present a peculiar memory effect observed in Fe_3O_4 nanoparticles using a unique FC aging protocol. This effect also provides a good measure for determining whether the system is a SPM or a SSG.¹² Figure 5 shows the memory effect of the FC magnetization which is measured in the following way. First, the system was cooled using the FC protocol from 298 K to intermittent stop temperatures T_s ($= 23, 20, 17, 14, 11, 8,$ and 5 K) in the presence of H ($= 5$ Oe). When the system was cooled down to each T_s , the field was turned off ($H = 0$) and the system was aged at T_s for a wait time t_s ($= 1.0 \times 10^4$ sec). The FC magnetization denoted by $M_{FC}^{IS}(T \downarrow)$ decreases with time t due to the relaxation, where IS stands for intermittent stop. After each wait time t_s at T_s , the field ($H = 5$ Oe) was turned on and the cooling was resumed. We find that such an aging process leads to a step-like behavior of $M_{FC}^{IS}(T \downarrow)$ curve. Immediately after reaching 2.0 K, the magnetization $M_{FC}^{IS}(T \uparrow)$ was measured in the presence of H ($= 5$ Oe) as the temperature was increased at a constant rate of 0.05 K/min. The magnetization $M_{FC}^{IS}(T \uparrow)$ thus measured exhibits step-like changes at each T_s . This implies that the spin configuration imprinted at each intermittent stop at T_s for the wait time t_s at $H = 0$ is retrieved by the curve on reheating. The magnetization $M_{FC}^{IS}(T \downarrow)$ is either parallel

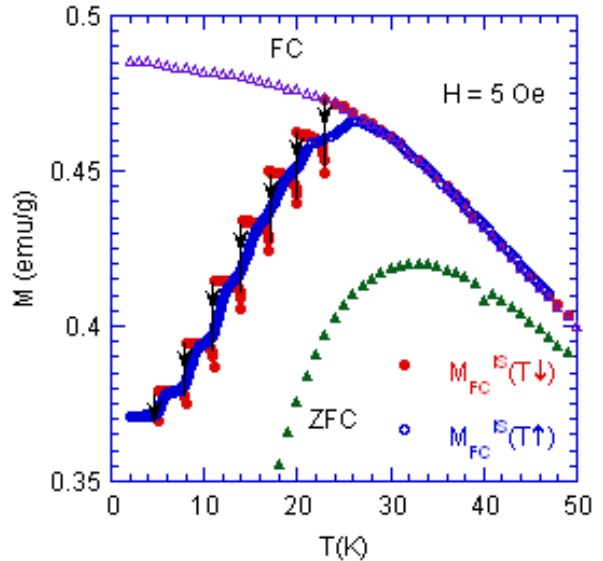


FIG. 5: (Color online) T dependence of $M_{FC}^{IS}(T \downarrow)$ (\bullet) and $M_{FC}^{IS}(T \uparrow)$ (\circ) for Fe_3O_4 nanoparticles, observed in the following FC aging protocol. The system is quenched from 298 to 50 K in the presence of H ($= 5$ Oe). $M_{FC}^{IS}(T \downarrow)$ is measured with decreasing T from 50 to 2.0 K but with intermittent stops (IS) at $T_s = 23, 20, 17, 14, 11, 8,$ and 5 K for a wait time $t_s = 1.0 \times 10^4$ sec. The field is cut off during each stop. The arrows indicate the relaxation of $M_{FC}^{IS}(T \downarrow)$. $M_{FC}^{IS}(T \uparrow)$ is measured at $H = 5$ Oe with increasing T after the above cooling process. The T dependence of M_{FC}^{ref} (Δ) and M_{ZFC}^{ref} (\blacktriangledown) are also shown as reference curves.

to M_{FC}^{ref} as a reference at temperatures near $T_s = 23$ and 20 K or is independent of T at temperatures near $T_s = 14, 11, 8,$ and 5 K. The magnetization $M_{FC}^{ref}(T \downarrow)$ without intermittent stops is almost constant well below T_f at $H = 5$ Oe. The magnetization $M_{FC}^{IS}(T \downarrow)$ with intermittent stops decreases with decreasing T , while $M_{FC}^{IS}(T \uparrow)$ increases with increasing T . They meet together at temperatures a little above each stop temperature (approximately 1 K). Similar memory effects in the FC magnetization have been observed in the SSG Fe_3N nanoparticles.¹² These features are in contrast to that of the SPM's such as ferritin (Sasaki et al.¹² and Mamiya et al.⁴), permalloy $\text{Ni}_{81}\text{Fe}_{19}$ (Sun et al.⁹), Co particles (Zheng et al.¹¹): both $M_{FC}^{IS}(T \downarrow)$ with intermittent stops and $M_{FC}^{ref}(T \downarrow)$ without intermittent stops monotonically increase with decreasing T .

In summary, the decrease of $M_{FC}^{IS}(T \downarrow)$ with decreasing T is a feature common to SSG's, while the increase of $M_{FC}^{IS}(T \downarrow)$ with decreasing T is a feature common to SPM's.

E. Memory effect in ZFC susceptibility

We measured the ZFC susceptibility of Fe_3O_4 nanoparticles after the ZFC aging protocol with a single-stop

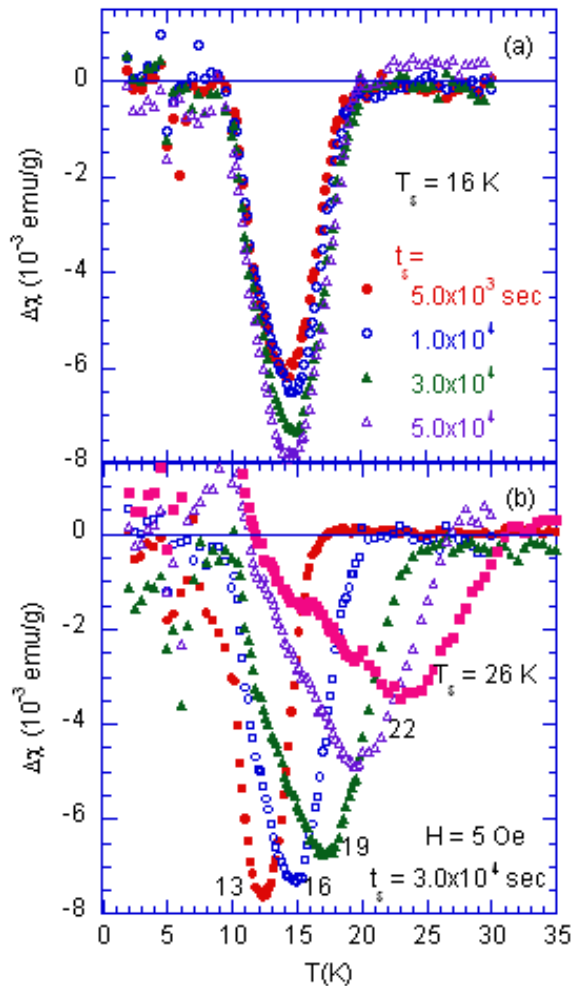


FIG. 6: (Color online) (a) T dependence of the genuine ZFC susceptibility for Fe_3O_4 nanoparticles. $\Delta\chi_{ZFC} = \chi_{ZFC}^{SSW}(T \uparrow) - \chi_{ZFC}^{ref}(T \uparrow)$. The system was annealed at $T = 100$ K for 1200 sec. After the system was quickly cooled from 100 K to a stop temperature T_s ($= 16$ K) at $H = 0$, it was aged at T_s for a wait time t_s ($= 5.0 \times 10^4$, 3.0×10^4 , 1.0×10^4 , 5.0×10^3 , and 2.0×10^3 sec) [single stop and wait (SSW) process]. The cooling was resumed from T_s to 2.0 K. Immediately after the field was turned on, the ZFC susceptibility $\chi_{ZFC}^{SSW}(T \uparrow)$ was measured at $H = 5$ Oe with increasing T . The reference ZFC susceptibility $\chi_{ZFC}^{ref}(T \uparrow)$ was measured at $H = 5$ Oe after the ZFC protocol without any stop and wait process. (b) T dependence of $\Delta\chi_{ZFC}$. $t_s = 3.0 \times 10^4$ sec. $T_s = 26$, 22, 19, 16, and 13 K. The ZFC protocol was the same as used in (a).

and wait (SSW) procedure. The sample was first rapidly cooled in zero-magnetic field from 100 K down to a stop temperature T_s . The system was aged at T_s for a wait time t_s . The cooling was then resumed down to 2.0 K. Immediately after the magnetic field was turned on, the ZFC susceptibility $\chi_{ZFC}^{SSW}(T \uparrow)$ was measured on reheating. The reference ZFC susceptibility $\chi_{ZFC}^{ref}(T \uparrow)$ was also measured after the direct cooling of the system from

100 to 2.0 K without any stop and wait process. Figure 6(a) shows the T dependence of the difference defined by $\Delta\chi_{ZFC} = \chi_{ZFC}^{SSW}(T \uparrow) - \chi_{ZFC}^{ref}(T \uparrow)$ for the SSW process, where $T_s = 16.0$ K and $H = 5$ Oe. The wait times are chosen as $t_s = 5.0 \times 10^3$, 1.0×10^4 , 3.0×10^4 , and 5.0×10^4 sec, respectively. We find that the difference $\Delta\chi_{ZFC}$ takes a local minimum (an aging dip) at 15.9 K just below T_s . When the system is isothermally aged at $T_s = 16.0$ K for t_s , its spin configuration gets arranged towards the equilibrium state. With further decrease in T , the equilibrated state becomes frozen in and the memory is retrieved on reheating. The depth of the aging dip is dependent on t_s , showing a clear evidence of the aging behavior that the domain size grows with time. We find here that the depth changes with increasing t_s according to a power law form given by

$$|\Delta\chi_{ZFC}^{SSW}|_{dip} = A t_s^b, \quad (7)$$

with $A = 0.0026 \pm 0.0002$ and $b = 0.10 \pm 0.01$. Similar time dependence of the aging dip has been observed in a 3D Ising SG $\text{Fe}_{0.5}\text{Mn}_{0.5}\text{TiO}_3$,²² where the depth of the aging dip logarithmically changes with t_s , rather than a power law form. We notice that our value of b is nearly equal to the exponent b'' obtained from the time dependence of the absorption $\chi''(\omega, t)$ ($= A'' t^{-b''}$) for $\text{Fe}_{0.5}\text{Mn}_{0.5}\text{TiO}_3$: $b'' = 0.14 \pm 0.03$.²³

Figure 6(b) shows the T dependence of the difference $\Delta\chi_{ZFC}$ at $H = 5$ Oe for the SSW process at T_s ($= 13$, 16, 19, 22, and 26 K) for a wait time t_s ($= 3.0 \times 10^4$ sec) during the ZFC protocol. The difference $\Delta\chi_{ZFC}$ clearly shows an aging dip. This dip occurs at the stop temperature T_s where the system is aged during the SSW process. This result indicates the occurrence of the aging behavior. The depth of the aging dip is the largest at $T_s = 13.0$ K and decreases with further increase in T_s . The width of the aging dip becomes broader as the stop temperature T_s increases for $13 \leq T_s \leq 26$ K. Since the aging dip is expected to disappear for T_s above T_f , this result indicates that the freezing temperature T_f is at least higher than $T_s = 26$ K. In fact, this result is consistent with our estimation of T_f ($= 30.6 \pm 1.6$ K) which is derived in Sec. III C. Similar T dependence of the aging dip has been observed in $\text{Fe}_{0.5}\text{Mn}_{0.5}\text{TiO}_3$ ²⁴ and canonical SG Ag (11 % at. % Mn).²⁴ Note that the detail of T dependence of the peak value and width of the aging dip may be rather different for different systems.

IV. DISCUSSION

In the mean-field picture, the phase transition of the SG systems can survive in the presence of low H , forming a critical line, the so-called de Almeida-Thouless (AT) line in the H - T phase diagram¹⁶

$$H(T) = H_0(1 - T/T_f)^p, \quad (8)$$

where T_f is the spin freezing temperature, H_0 is a field amplitude and the exponent $p = 3/2$. This line is the

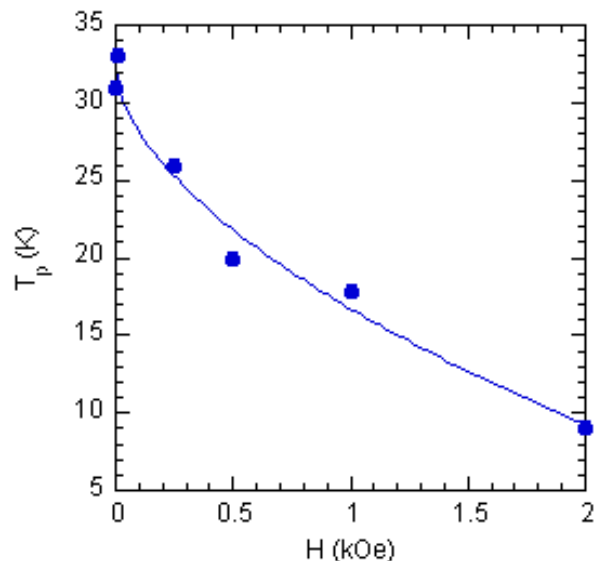


FIG. 7: (Color online) Plot of T_p as a function of H for Fe_3O_4 nanoparticles. T_p is a temperature at which χ_{ZFC} exhibits a peak. The solid line is least-squares fitting curve to Eq. (8) with $T_f = 32.5 \pm 1.4$ K, $H_0 = 3.61 \pm 0.71$ kOe, and $p = 1.78 \pm 0.36$.

phase boundary between the PM (paramagnetic) phase and the SG phase. The correlation length and relaxation times diverge on crossing this line. In Fig. 7 we show the plot of the ZFC-peak temperature T_p of χ_{ZFC} vs T as a function of H for Fe_3O_4 nanoparticles. The peak temperature T_p decreases with increasing H . This critical line in the H - T_p diagram may correspond to the phase boundary between the SPM and SSG phases. The least-squares fit of the data of H vs T_p for $1 \text{ Oe} \leq H \leq 2$ kOe to Eq. (8) yields the parameters $p = 1.78 \pm 0.26$, $T_f = 32.5 \pm 1.4$ K, and $H_0 = 3.61 \pm 0.71$ kOe. We find that p is close to the AT exponent ($p = 3/2$). These results indicate that there is an AT critical line in the H - T phase diagram for Fe_3O_4 nanoparticles as a SSG system. Here we note that similar AT critical line has been reported by Sahoo et al.⁷ for ferromagnetic single domain particles of CoFe in discontinuous magnetic layers ($\text{Co}_{80}\text{Fe}_{20}/\text{Al}_2\text{O}_3$ multilayers). This system undergoes a SSG transition at a spin freezing temperature T_f . The peak temperature

T_p of the ZFC susceptibility shifts to the low- T side with increasing H . The least-squares fit of the data of T_p vs H in the low-field range to Eq. (8) yields the exponent p ($= 1.5 \pm 0.4$), which is close to the AT exponent ($p = 3/2$). In conclusion, the nature of the AT line in SSG systems is essentially the same as that in the SG systems.

The above discussion is based on the mean-field picture. The situation is rather different in the droplet picture.²⁵ It is predicted that no phase transition occurs in the presence of even an infinitesimal H as in the case of a ferromagnet. So there is no AT line in the H - T phase diagram. Any apparent transition would be an artifact related to the limited experimental time scale. Several experimental results support the prediction from the droplet picture; the instability of the SG phase in thermal equilibrium in a finite H .^{26,27}

V. CONCLUSION

The aging and memory effects of Fe_3O_4 nanoparticles have been studied in a series of DC magnetization measurements using various cooling protocols. The genuine FC magnetization after the FC procedure with multiple intermittent stop and wait processes shows a step-like increase at each stop temperature on reheating. The genuine ZFC magnetization after the ZFC procedure with a single intermittent stop and wait process shows an aging dip at the stop temperature on reheating. The depth of the aging dip is dependent on the wait time. The frequency dependence of the AC magnetic susceptibility for Fe_3O_4 nanoparticles is indicative of critical slowing down at a freezing temperature T_f ($= 30.6 \pm 1.6$ K). The flatness of the FC susceptibility is observed below the ZFC-peak temperature T_p . The H dependence of T_p for Fe_3O_4 nanoparticles forms a critical line with an exponent $p = 1.78 \pm 0.26$, close to the de Almeida-Thouless exponent ($= 3/2$). These results are well described by the SSG model of interacting Fe_3O_4 nanoparticle system.

Acknowledgments

The preparation of nanomaterials was supported by National Science Foundation (CHE 0349040).

* suzuki@binghamton.edu

¹ T. Jonsson, J. Mattsson, C. Djurberg, F. A. Khan, P. Nordblad, and P. Svedlindh, Phys. Rev. Lett. **75**, 4138 (1995).

² C. Djurberg, P. Svedlindh, P. Nordblad, M. F. Hansen, F. Bødker, and S. Mørup, Phys. Rev. Lett. **79**, 5154 (1997).

³ T. Jonsson, P. Svedlindh, and M. F. Hansen, Phys. Rev. Lett. **81**, 3976 (1998).

⁴ H. Mamiya, I. Nakatani, and T. Furubayashi, Phys. Rev. Lett. **80**, 177 (1998).

⁵ P. Jönsson, M. F. Hansen, and P. Nordblad, Phys. Rev. B **61**, 1261 (2000).

⁶ M. F. Hansen, P. E. Jönsson, P. Nordblad, and P. Svedlindh, J. Phys.: Condens. Matter **14**, 4901 (2002).

⁷ S. Sahoo, O. Petravic, Ch. Binek, W. Kleemann, J. B. Sousa, S. Cardoso, and P. P. Freitas, Phys. Rev. B **65**, 134406 (2002).

⁸ S. Sahoo, O. Petravic, W. Kleemann, P. Nordblad, S. Cardoso, and P. P. Freitas, Phys. Rev. B **67**, 214422 (2003).

⁹ Y. Sun, M. B. Salamon, K. Garnier, and R. S. Averback,

- Phys. Rev. Lett. **91**, 167206 (2003).
- ¹⁰ S. Sahoo, O. Petravic, W. Kleemann, P. Nordblad, S. Cardoso, and P. P. Freitas, *J. Magn. Magn. Mater.* **272-276**, 1316 (2004).
- ¹¹ R. K. Zheng, G. Hongwei, and X. X. Zhang, *Phys. Rev. Lett.* **93**, 139702 (2004).
- ¹² M. Sasaki, P. E. Jönsson, H. Takayama, and H. Mamiya, *Phys. Rev. B* **71**, 104405 (2005).
- ¹³ G. M. Tsoi, L. E. Wenger, U. Senaratne, R. J. Tackett, E. C. Buc, R. Naik, P. P. Vaishnava, and V. Naik, *Phys. Rev. B* **72**, 014445 (2005).
- ¹⁴ L. Wang, J. Luo, M. Maye, Q. Fan, Q. Rendeng, M. Engelhard, C. Wang, Y. Lin, and C. J. Zhong, *J. Mater. Chem.* **15**, 1821 (2005).
- ¹⁵ L. Wang, J. Luo, Q. Fan, M. Suzuki, I. S. Suzuki, M. H. Engelhard, Y. Lin, N. Kim, J. Q. Wang, and C. J. Zhong, *J. Phys. Chem. B* **109**, 21593 (2005).
- ¹⁶ J. R. L. de Almeida and D. J. Thouless, *J. Phys. A* **11**, 983 (1978).
- ¹⁷ C. Kittel, *Introduction to Solid State Physics*, 7-th ed. (John Wiley & Sons, New York, 1966).
- ¹⁸ M. Matsubara, Y. Shimada, T. Arima, Y. Taguchi, and Y. Tokura, *Phys. Rev. B* **72**, 220404(R) (2005).
- ¹⁹ L.R. Bickford, Jr., *Phys. Rev.* **76**, 137 (1949).
- ²⁰ J. A. Mydosh, *Spin glasses: an experimental introduction* (Taylor & Francis, London, 1993).
- ²¹ K. Gunnarsson, P. Svedlindh, P. Nordblad, L. Lundgren, H. Aruga, and A. Ito, *Phys. Rev. Lett.* **61**, 754 (1988).
- ²² R. Mathieu, P. E. Jönsson, P. Nordblad, H. A. Katori, and A. Ito, *Phys. Rev. B* **65**, 012411 (2001).
- ²³ V. Dupuis, E. Vincent, J.-P. Bouchaud, J. Hammann, A. Ito, and H. A. Katori, *Phys. Rev. B* **64**, 174204 (2001).
- ²⁴ P. E. Jönsson, R. Mathieu, P. Nordblad, H. Yoshino, H. A. Katori, and A. Ito, *Phys. Rev. B* **70**, 174402 (2004).
- ²⁵ D. S. Fisher and D. A. Huse, *Phys. Rev. Lett.* **56**, 1601 (1986); *Phys. Rev. B* **38**, 373 (1988); *Phys. Rev. B* **38**, 386 (1988).
- ²⁶ J. Mattsson, T. Jonsson, P. Nordblad, H. A. Katori, and A. Ito, *Phys. Rev. Lett.* **74**, 4305 (1995).
- ²⁷ I. S. Suzuki and M. Suzuki, *Phys. Rev. B* **72**, 104429 (2005).